ORIGINAL RESEARCH

Silica nanoparticles induce liver fibrosis via TGF-β$_I$/Smad3 pathway in ICR mice

Yang Yu[1,2]
Junchao Duan[1,2]
Yang Li[1,2]
Yanbo Li[1,2]
Li Jing[1,2]
Man Yang[1,2]
Ji Wang[1,2]
Zhiwei Sun[1,2]

[1]School of Public Health, Capital Medical University, Beijing, People's Republic of China; [2]Beijing Key Laboratory of Environmental Toxicology, Capital Medical University, Beijing, People's Republic of China

Correspondence: Zhiwei Sun
School of Public Health, Capital Medical University, Beijing, 100069, People's Republic of China
Tel +86 10 8391 1507
Fax +86 10 8391 1507
Email zwsun@ccmu.edu.cn

Abstract: The liver is one of the target organs of silica nanoparticles (SiO$_2$ NPs) but the toxic mechanism on the liver still remains unclear. This study aimed to explore the hepatic toxicity and its mechanism through repeated intravenous exposure to SiO$_2$ NPs in ICR mice. Results indicated that SiO$_2$ NPs could be distributed in hepatocytes, Kupffer cells, and hepatic stellate cells, and induce hepatic dysfunction as well as granuloma formation in the liver. The increase of lipid peroxide level and decrease of antioxidant enzyme activities in the liver indicated that SiO$_2$ NPs could induce hepatic oxidative damage. SiO$_2$ NPs induced hepatocytes' apoptosis shown by morphological examination and TUNEL assay. The results of Masson's trichrome staining and hydroxyproline assay showed hyperplasia of collagen fibers in the liver, suggesting SiO$_2$ NPs caused liver fibrosis, and it was promoted by oxidative damage and hepatocytes' apoptosis. The results of Western blot analysis and immunohistochemical staining indicated that the activation of TGF-β$_1$/Smad3 signaling pathway played an important role in this pathophysiological process. The results suggested that oxidative damage and hepatocyte apoptosis activated TGF-β$_1$/Smad3 signaling pathway, and thus promoted the process of liver fibrosis induced by intravenous injection of SiO$_2$ NPs in mice. This study, for the first time, investigated liver fibrosis and its related mechanism induced by repeated intravenous exposure of amorphous SiO$_2$ NPs, and provides important experimental evidence for safety evaluation of SiO$_2$ NPs, especially in biomedical application.

Keywords: silica nanoparticles, oxidative stress, hepatocyte apoptosis, fibrosis, TGF-β$_1$/Smad3 signaling pathway

Introduction

Silica nanoparticles' (SiO$_2$ NPs') output is the largest in engineering nanomaterials because of its stable physical-chemical properties and good biocompatibility, and are widely used in drug delivery, biological imaging, and medical diagnosis, etc. In the field of biomedical application, as drug carrier, SiO$_2$ NPs enter into the body by intravenous injection; in the food processing industry, average daily intake of SiO$_2$ NPs as food additive in the human body reaches 1.8 mg/kg;[1] an environmental study has shown that SiO$_2$ NPs are an important inorganic composition of atmospheric pollution;[2] in occupational exposure, SiO$_2$ NPs could enter the lung by respiration and then pass the gas-blood barrier into systemic circulation. Thus, with the application increasing and environmental pollution exaggerated, the population's exposure to SiO$_2$ NPs is apparently increased. SiO$_2$ NPs are on the priority list of manufactured nanomaterials for toxicological evaluation by Organisation for Economic Co-operation and Development,[3] so attention should be paid to the hazard of SiO$_2$ NPs to environmental safety and human health.

As an important part of the reticuloendothelial system, the liver has the responsibility of recognition and clearance of nanoparticles which have entered into the

bloodstream.[4,5] Toxicokinetics study also indicated that the liver was the largest holder for nanoparticles by intravenous injection.[6] So, the liver could be the primary target organ through intravenous administration of SiO$_2$ NPs. Previously, we reported the acute toxicity of SiO$_2$ NPs by intravenous injection in mice, and SiO$_2$ NPs could also induce elevation of serum AST level in a dose-dependent manner.[7] Several studies have also demonstrated that SiO$_2$ NPs may be hepatotoxic by intravenous injection in animal models.[8,9]

van der Zande et al observed that rats orally exposed to SiO$_2$ NPs, showed significantly elevated expression of fibrosis-related genes in the liver, their study provided us with an important clue that SiO$_2$ NPs may induce liver fibrosis through oral administration.[10] Few studies have investigated the toxicity of SiO$_2$ NPs on the liver by intravenous administration. Liu et al reported that mesoporous SiO$_2$ NPs could induce hepatic fibrosis in intravenously exposed mice.[11] So far it is still indistinct whether amorphous SiO$_2$ NPs could induce liver fibrosis after intravenous injection, and the related mechanism is also unknown. Due to more and more biomedical application of SiO$_2$ NPs, it is important to clarify the hepatic toxicity of SiO$_2$ NPs in intravenous exposure.

So this study plans to evaluate the hepatic toxicity of SiO$_2$ NPs and preliminarily explore the related mechanism by repeated intravenous exposure in mice. Blood biochemical indexes were used to assess the impairment of liver function. Hepatic morphological changes, ultrastructural changes, and ultra-distribution of SiO$_2$ NPs were observed. Oxidative damage and cell apoptosis were used to assess liver injury. The collagen fiber content was tested to assess liver fibrosis. The activation of TGF-β$_1$/Smad3 pathway was detected to confirm its participation in the process of liver fibrosis induced by SiO$_2$ NPs. This study observes the liver injury not only immediately after repeated intravenous exposure, but also after 45-day recovery period, so as to provide more comprehensive understanding of hepatic injury induced by SiO$_2$ NPs.

Methods
SiO$_2$ NPs' preparation and characterization
The amorphous SiO$_2$ NPs were prepared using the Stöber method as previously described.[12] The SiO$_2$ NPs were dispersed in distilled water (stock media) or saline (exposure media) at the concentration of 500 µg/mL. The SiO$_2$ NPs drop was added to the copper grid and put in the incubators at 50°C for 24 h. Then, the shape and size of SiO$_2$ NPs were observed by transmission electron microscopy (TEM) (JEM2100; JEOL, Akishima-shi, Japan). The zeta potential and hydrodynamic sizes of SiO$_2$

NPs in dispersion media at the concentration 500 µg/mL were measured by zeta electric potential granulometer (Nano-ZS90; Malvern Instruments, Malvern, UK). The purity of the SiO$_2$ NPs was determined by inductively coupled plasma-atomic emission spectrometer (ARL 3520; ARL, Washington, DC, USA). The endotoxin detection was conducted using Gel-Clot Limulus Amebocyte Lysate (LAL) assay (Bokang, Zhanjiang, Guangdong, People's Republic of China).

Animals
Male ICR mice (8 weeks old with weight 20–22 g) were purchased from Vital River Laboratory Animal Technology Co. Ltd (Beijing, People's Republic of China). Groups of five mice were kept in a stainless steel cage. They were allowed to have free access to water and chow in a temperature controlled room (20°C±2°C) with 60%±10% relative humidity and a 12:12 h light/dark cycle. Prior to the final treatment, the mice were fasted overnight. The experiment followed the National Guidelines for Animal Care and Use, and was approved by the Laboratory Animal Care and Use Committee in Capital Medical University.

The mice were continuously intravenously injected with SiO$_2$ NPs at 20 mg/kg once every 3 days, in total five times. The dosage selection of SiO$_2$ NPs was based on our previous acute toxicity study.[7] An amount of 20 mg/kg is not only less than one tenth of the LD50 of SiO$_2$ NPs, but also lower than the lowest level in previous acute toxicity study. The control groups were intravenously injected with the same volumes of sterile saline. Mortality and clinical manifestation was recorded. The mice were sacrificed at days 15, 30, and 60 after the first injection, and the serum and livers were harvested for further study, the experimental design was shown in Figure 1. The livers were weighed accurately, and the coefficients of livers were calculated as the ratio of livers (wet weight, mg) to body weight (g).

Blood biochemical assay
Blood samples were collected via the ocular vein. The serum was obtained by centrifugation of the whole blood at
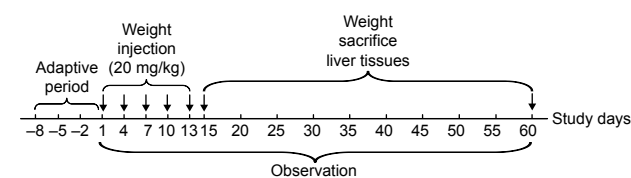

Figure 1 Experimental design of SiO$_2$ NPs induced liver fibrosis via TGF-β$_1$/Smad3 pathway in ICR mice. The arrows denote days of SiO$_2$ NPs injection from day 1 to day 13, or days mice sacrificed from day 15 to day 60.
Abbreviation: SiO$_2$ NPs, silica nanoparticles.

3,000 rpm for 15 min. The serum levels of AST, ALT, LDH, and ALB were assayed by an automated biochemical analyzer (Type 7200-202; Hitachi Ltd., Tokyo, Japan).

Histopathological examination

The livers were fixed in 10% formalin, embedded in paraffin, sectioned, and stained with hematoxylin and eosin for histological examination. After staining, the histopathological changes were observed and examined under optical microscope (Olympus X71-F22PH; Olympus Corporation, Tokyo, Japan). For quantification, the total number and size of granulomas in 30 optical fields (200× magnification) of each liver section were determined using the Olympus software (CellSens Standard). The fields were chosen randomly and continuously. Data were presented as mean ± SD of five mice of each group. The pathologist was blinded to all the histopathological examinations.

TEM imaging

The livers were excised and immediately fixed in 3% glutaraldehyde overnight. Then the samples were rinsed three times with 0.1 M PBs and postfixed with 1% osmic acid for 2 h. After being rinsed three times with 0.1 M PB and serially dehydrated with 50%, 70%, 80%, 90%, and 100% alcohol and 100% acetone, the samples were embedded in epoxy resin. The ultrathin sections (50 nm) were obtained by an ultra-microtome (Ultra cut UCT; Leica Microsystems, Wetzlar, Germany). They were then stained with lead citrate and uranyl acetate, and observed by TEM. The pathologist was blinded to identity and analysis of the ultrathin sections.

Assessment of oxidative damage

The oxidative damage in the liver was assessed by measuring the level of MDA as an end product of lipid peroxidation, the activities of SOD and GSH-Px as the anti-oxidative systems to eliminate ROS. Liver tissues (100 mg) were homogenized in 1 mL ice-cold saline. After centrifuging the homogenates at 3,000 rpm at 4°C for 10 min, the supernatants were collected for measurement of the production of MDA, the activities of SOD and GSH-Px at concentrations of 10%, 5%, and 1%, respectively. All examinations were carried out using commercially available kits (Jiancheng, Nanjing, Jiangsu, People's Republic of China) according to the manufacturer's instructions. The protein concentrations of the liver homogenates were determined by the BCA protein assay (Jiancheng).

Apoptosis detection by TUNEL stain

In situ detection of DNA fragmentation was performed using TUNEL staining on liver paraffin sections in mice. In apoptosis the cleavage of DNA by endogenous DNases leads to the formation of free 3′ DNA hydroxyl groups, which are substrates for the enzyme TdT that can attach nucleotides to the free 3′ DNA hydroxyl groups. In TUNEL staining, labeled nucleotides represent the cells undergoing apoptosis. TUNEL staining was performed according to an in situ cell death detection kit (KeyGEN, Nanjing, Jiangsu, People's Republic of China) following the manufacturer's protocol.

Detection of collagen content

Liver paraffin sections were stained by Masson's trichrome stains[13] to assess liver fibrosis. The slides were observed using an optical microscope (Olympus X71-F22PH). Slides showed red keratin and muscle fibers, blue or green collagen and bone, light red or pink cytoplasm, and dark brown cell nuclei.

Hepatic hydroxyproline (HYP) content in the liver was measured by Kivirikko's method with some modification[14] by using HYP assay kits (Jiancheng). The results were expressed as mg of hydroxyproline per g of wet liver weight.

Western blot analysis

The total protein was extracted with the Tissue Total Protein Extraction Kit (KeyGEN) and determined using the BCA protein kit (Jiancheng) according to the manufacturer's instructions. Equal amounts of lysate proteins (40 µg) were loaded onto SDS-polyacrylamide gels (12% separation gels) and electrophoretically transferred to PVDF membranes (EMD Millipore, Billerica, MA, USA). The membrane was blocked with fat-free milk at room temperature for 2 h and incubated at 4°C overnight with the following primary antibodies: TGF-β₁ (Abcam, Cambridge, MA, USA), Smad3, p-Smad3, and β-actin (Cell Signaling Technology [CST], Beverly, MA, USA) in 5% fat-free milk in TBST separately. The membranes were washed with TBST three times, each time for 10 min and incubated with 1:2,000 dilution of HRP-conjugated secondary antibody (CST) at room temperature for 1 h. After being washed three times with TBST, the antibody-bound proteins were detected using the enhanced chemiluminescence reagent (Thermo Fisher Scientific, Waltham, MA, USA).

Immunohistochemical staining

p-Smad3 was detected immunohistochemically in the paraffin-embedded liver sections. After deparaffinization

and rehydration, the liver sections were placed in a 10 mM citrate buffer solution (pH 6.0) for antigen retrieval. In order to quench endogenous peroxidase activity, the sections were treated with 3% H_2O_2 in PBS for 5 min and then washed in PBS. Then, the sections were blocked with 10% normal goat serum at 37°C for 10 min and incubated with primary antibody or an equivalent amount of normal goat IgG as a negative control at 4°C overnight. The sections were then treated with an avidin-biotin affinity system at room temperature for 30 min, stained with 3-3′ diaminobenzidine substrate, and counter-stained with hematoxylin. The pathologist was blinded to all the analyses of the slides. A brown staining indicates positive expression. Results were expressed as the total positive cell numbers from 50 random and continuous fields in each section.

Statistical analysis

Results were expressed as mean ± SD. Significance was determined by using one-way ANOVA and followed by least significant difference test to compare the differences between groups. Independent sample t-test was performed to compare the difference between control group and the SiO_2 NPs treated groups at the same time. Differences were considered significant at $P<0.05$.

Results
Characterization of SiO_2 NPs

The SiO_2 NPs were well characterized in our previous research.[7,15] The average size of the spherical SiO_2 NPs was 64.43±10.50 nm and the SiO_2 NPs had good monodispersity in distilled water and in saline with time. In addition, the SiO_2 NPs' purity was >99.9% and the LAL assay indicated no detectable gram negative endotoxin.

Weight gain and coefficient of livers

As shown in Figure 2, the total weight gain decreased in a time-dependent manner in the control and in the SiO_2 NPs treated mice, and the values in the SiO_2 NPs treated mice were lower than in the control groups, with significant difference at day 15 and day 60 ($P<0.05$). Besides, SiO_2 NPs induced hepatomegaly in mice. The coefficients of livers were significantly increased in the SiO_2 NPs treated groups than that in the control groups at days 15, 30, and 60. The coefficients of livers in the SiO_2 NPs treated group decreased in the period of observation but were still significantly higher than in the control group at day 60 (Figure 2).

Blood biochemical assay

SiO_2 NPs induced serum ALT and AST elevation in the SiO_2 NPs treated groups as shown in Figure 3. Also, the level of serum LDH significantly increased in the SiO_2 NPs treated groups compared with the control groups. The levels of serum ALT, AST, and LDH in the SiO_2 NP treated mice were all first elevated at day 15, and then reached the peak value at day 30, and finally decreased at day 60. But at day 60, the AST level and LDH level still remained higher in the SiO_2 NP treated groups than that in the control groups ($P<0.05$). The levels of serum ALB and A/G in the SiO_2 NPs treated groups decreased in a time-dependent manner, and the A/G was significantly lower than that in the control group at day 60 ($P<0.05$). On the other hand, the serum GLB level was significantly elevated in the SiO_2 NP treated groups compared with that in the control group at day 60.

Pathological examination

SiO_2 NPs induced lymphocytic infiltration, granuloma formation, and hepatocellular hydropic degeneration in the liver
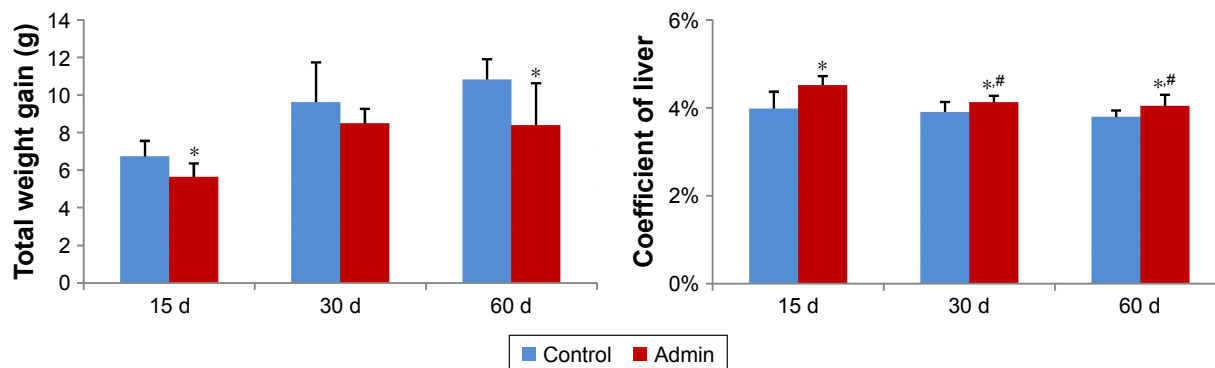

Figure 2 Total weight gain and coefficient of livers of mice at days 15, 30, and 60.
Notes: Data are expressed as mean ± SD (n=8 or 10). *$P<0.05$ compared with control group using independent sample t-test, #$P<0.05$ compared with SiO_2 NPs treated group at day 15 using ANOVA and LSD.
Abbreviations: Admin, administration; SiO_2 NPs, silica nanoparticles; LSD, least significant difference.
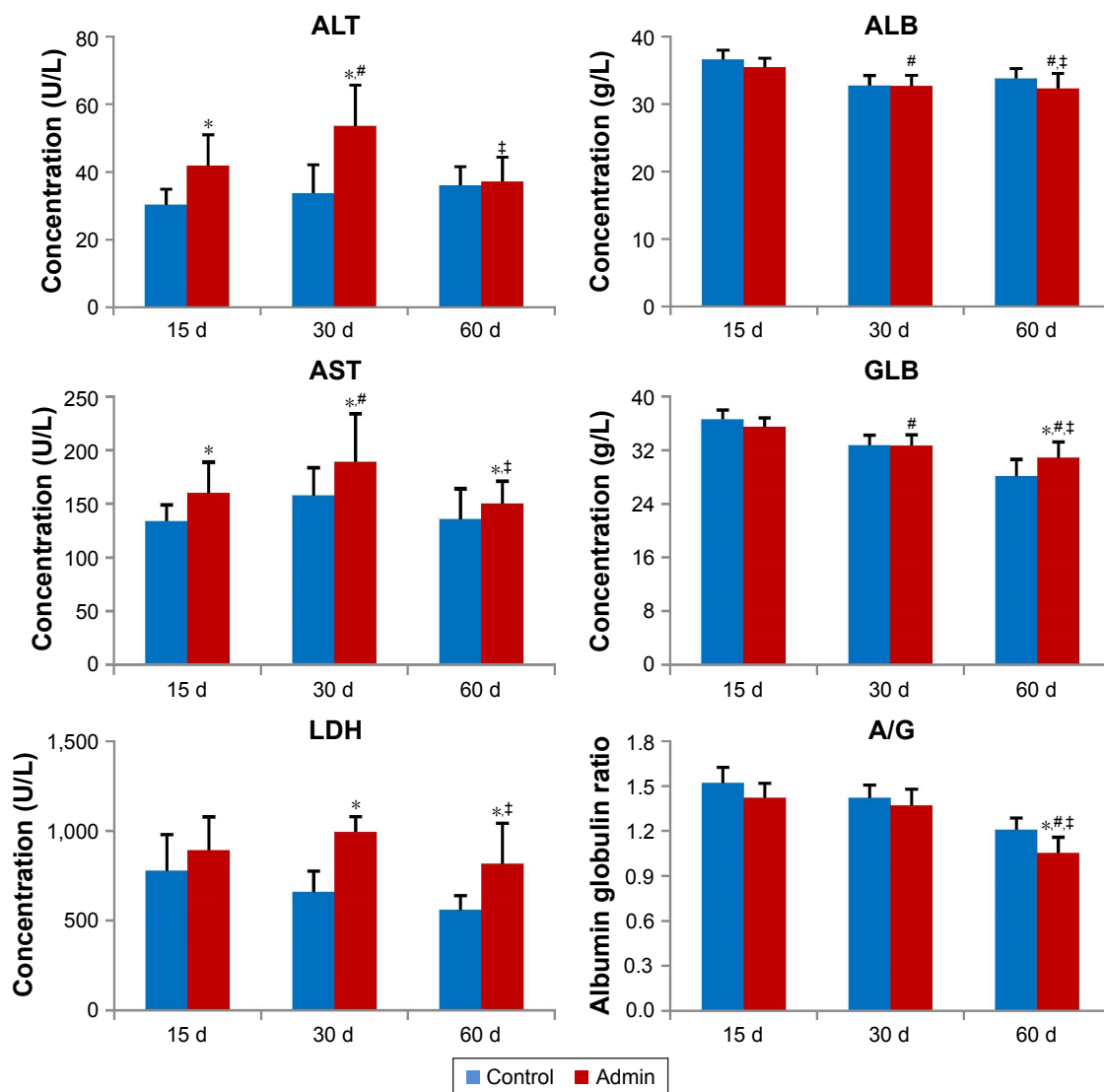
Figure 3 Blood biochemical index of the mice treated with SiO₂ NPs at days 15, 30, and 60.
Notes: Data are expressed as mean ± SD (n=8 or 10). *$P<0.05$ compared with control group using independent sample t-test, #$P<0.05$ compared with SiO₂ NP treated group at day 15, ‡$P<0.05$ compared with SiO₂ NP treated group at day 30 using ANOVA and LSD.
Abbreviations: Admin, administration; SiO₂ NPs, silica nanoparticles; LSD, least significant difference.

samples of mice at days 15, 30, and 60 (Figure 4A). The liver sections exhibited well-formed multi-cellular granulomas with a large number of macrophages and minimal hepatocyte necrosis, as well as inflammatory cell infiltration in the SiO₂ NP treated mice at day 15 and day 30. In contrast, the granulomas in the liver sections in the SiO₂ NP treated mice at day 60 appeared more collagen fibers which were stained pink (Figure 4A). In addition, hepatic sinusoid and central vein hyperemia, hepatocyte degeneration, apoptosis, and necrosis were also observed in the liver sections in the SiO₂ NP treated mice (Figure 4A). The numbers, total sizes, and average sizes of granulomas in the livers in the SiO₂ NP treated mice decreased in a time-dependent manner (Figure 4B). The total sizes of granulomas in the livers in the

SiO₂ NP treated mice at day 15 were respectively 1.8-fold and 5.8-fold larger than that in the livers from the SiO₂ NP treated mice at day 30 and day 60.

TEM imaging

The ultrastructural distribution of SiO₂ NPs was shown in Figure 5. SiO₂ NPs were mainly distributed in the Kupffer cells (KCs) and macrophages (Figure 5A and C), while a few SiO₂ NPs were trapped in the hepatocytes, the hepatic stellate cells (HSCs), and the fibroblast cells (Figure 5E, I, and K). Besides, a large amount of SiO₂ NPs were trapped in the inflammatory cells such as the neutrophils in the granulomas (Figure 5G). SiO₂ NPs mainly persisted in membrane-enclosed vesicles called lysosomes in the cells.
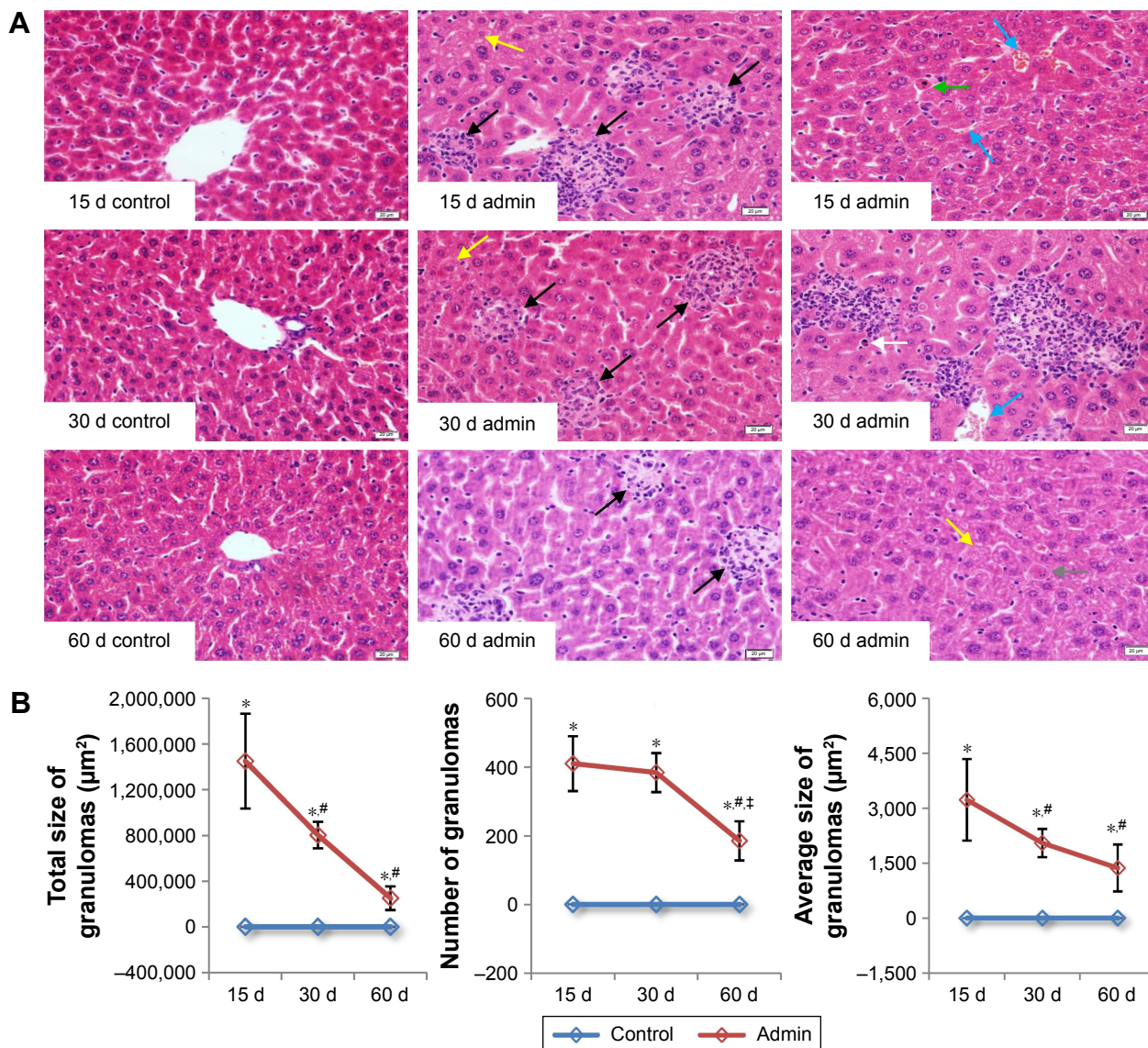
Figure 4 Histological analyses of liver of the SiO$_2$ NP treated mice.

Notes: (**A**) Representative liver sections taken from the control mice and SiO$_2$ NP treated mice at days 15, 30, and 60 at 400× magnification. Granulomas and lymphocytic infiltration (black arrows) in the liver, hydropic degeneration in hepatocytes (yellow arrows), hepatic sinusoid and central vein hyperemia (blue arrows), hepatocyte apoptosis (green arrow), eosinophilia infiltration (white arrow), and hepatocyte degeneration and necrosis (gray arrow) was observed in the liver of the SiO$_2$ NP treated mice. (**B**) The total size, number, and average size of granulomas in the SiO$_2$ NP treated mice at days 15, 30, and 60. Data are expressed as mean ± SD (n=8 or 10). *$P<0.05$ compared with control group using independent sample t-test, #$P<0.05$ compared with SiO$_2$ NP treated group at day 15, ‡$P<0.05$ compared with SiO$_2$ NP treated group at day 30 using ANOVA and LSD. Data are representative of at least eight mice. Scale bar =20 μm.

Abbreviations: admin, administration; SiO$_2$ NPs, silica nanoparticles; LSD, least significant difference.

Figure 6 showed the abnormal ultrastructural changes in the liver in the SiO$_2$ NP treated mice. The hepatocytes in the SiO$_2$ NP treated mice appeared typical morphological changes of apoptosis, such as distorted nuclear membrane, increased nuclear membrane indentation with chromatin margination, crescent-shaped nucleus, condensation of mitochondria, and lipid droplet accumulation in the cytoplasm as well as vacuolization (Figure 6A, D, and G). Figure 6 also showed the typical changes of the granuloma with time. Firstly, several KCs aggregated together with the infiltration of the inflammatory cells, and led to the cellular granuloma formation at

day 30 (Figure 6E), which turned out to be a fibrosis granuloma at day 60 with SiO$_2$ NPs in the center and surrounded by a large amount of collagen fibers as well as fibroblast proliferation (Figure 6H). Additionally, nuclear condensation, lamellar body-like structure, vacuolization (Figure 6E), and cell necrosis and apoptosis was also observed in the cellular granuloma.

Oxidative damage assessment

Figure 7 showed the results of evaluation of the oxidative damage in the liver by intravenous administration of SiO$_2$
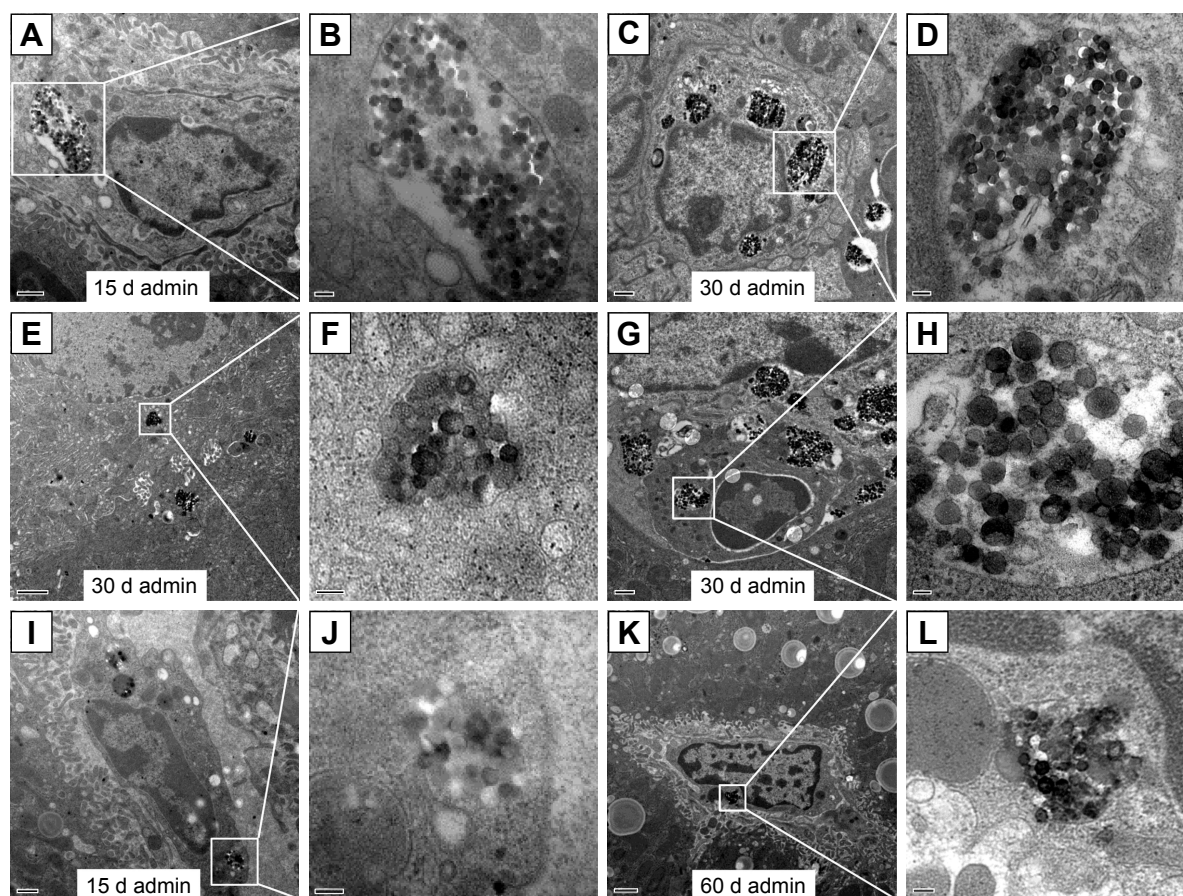
Figure 5 TEM images of the distribution of SiO₂ NPs in the liver of mice at days 15, 30, and 60.
Notes: The regions in the white boxes denote phagolysosomes with endocytosed SiO₂ NPs and are magnified on the right-hand side of each image.(**A**, **B**) SiO₂ NPs in the Kupffer cells in the liver (15 k, 50 k), (**C**, **D**) SiO₂ NPs in the macrophages in the granuloma (10 K, 50 k), (**E**, **F**) SiO₂ NPs in the hepatocytes (8 K, 80 k), (**G**, **H**) SiO₂ NPs in the neutrophils in the granuloma (10 K, 50 k), (**I**, **J**) SiO₂ NPs in the hepatic stellate cells (12 K, 80 k), (**K**, **L**) SiO₂ NPs in the fibroblast cells in the liver (6 K, 60 k). Scale bars: (**A**) 0.5 μm; (**B**) 100 nm; (**C**) 0.5 μm; (**D**) 100 nm; (**E**)1 μm; (**F**) 100 nm; (**G**) 0.5 μm; (**H**) 50 nm; (**I**) 0.5 μm; (**J**) 100 nm; (**K**) 1 μm; (**L**) 100 nm.
Abbreviations: admin, administration; TEM, transmission electron microscopy; SiO₂ NPs, silica nanoparticles.

NPs in mice. As a product of lipid peroxidation, the MDA level in the liver in the SiO₂ NP treated mice increased significantly compared with that in the control groups ($P<0.05$) at day 15 and day 30, and was 2.35-fold and 1.83-fold higher than that in the control groups, respectively. The MDA level was also higher than that in the control group at day 60 but with no significant difference. On the contrary, the defense systems against free radical attack, the activities of SOD and GSH-Px in the liver in the SiO₂ NP treated mice both decreased at day 15 and day 30, and recovered at day 60. But only the activities of SOD and GSH-Px in the liver in the SiO₂ NP treated mice decreased significantly compared with control group at day 15 ($P<0.05$).

Cell apoptosis detection

The DNA fragments in apoptotic cells were detected using the TUNEL assay. In the liver sections of control mice, the apoptotic cells were occasionally observed in the hepatic sinusoid and were mainly KCs (Figure 8A). In the SiO₂ NP treated mice, a large amount of apoptotic cells were observed in the

liver section, including hepatocytes in the liver parenchyma, KCs in the hepatic sinusoid, and KCs as well as inflammatory cells in the granulomatous lesion (Figure 8A). The positive cell numbers in the liver section decreased in a time-dependent manner in SiO₂ NP treated mice (Figure 8B).

Measurement of collagen fibers

Histopathological changes of fibrosis occurring in the SiO₂ NP treated mice were shown in Figure 9A. The livers of mice treated with SiO₂ NPs showed extensive accumulation of connective tissue resulting in the formation of continuous fibrotic septa, nodules of regeneration, and noticeable alterations in the central vein and around granulomatous lesions (Figure 9A), which was also observed under TEM (Figure 6). The hydroxyproline content, the marker of collagen accumulation, was elevated in the liver in the SiO₂ NP treated mice, in the meantime the results indicated that the extent of fibrosis was aggravated in a time-dependent manner, and SiO₂ NPs induced the HYP content which was elevated to 1.4-fold compared with control values at day 60 (Figure 9B).
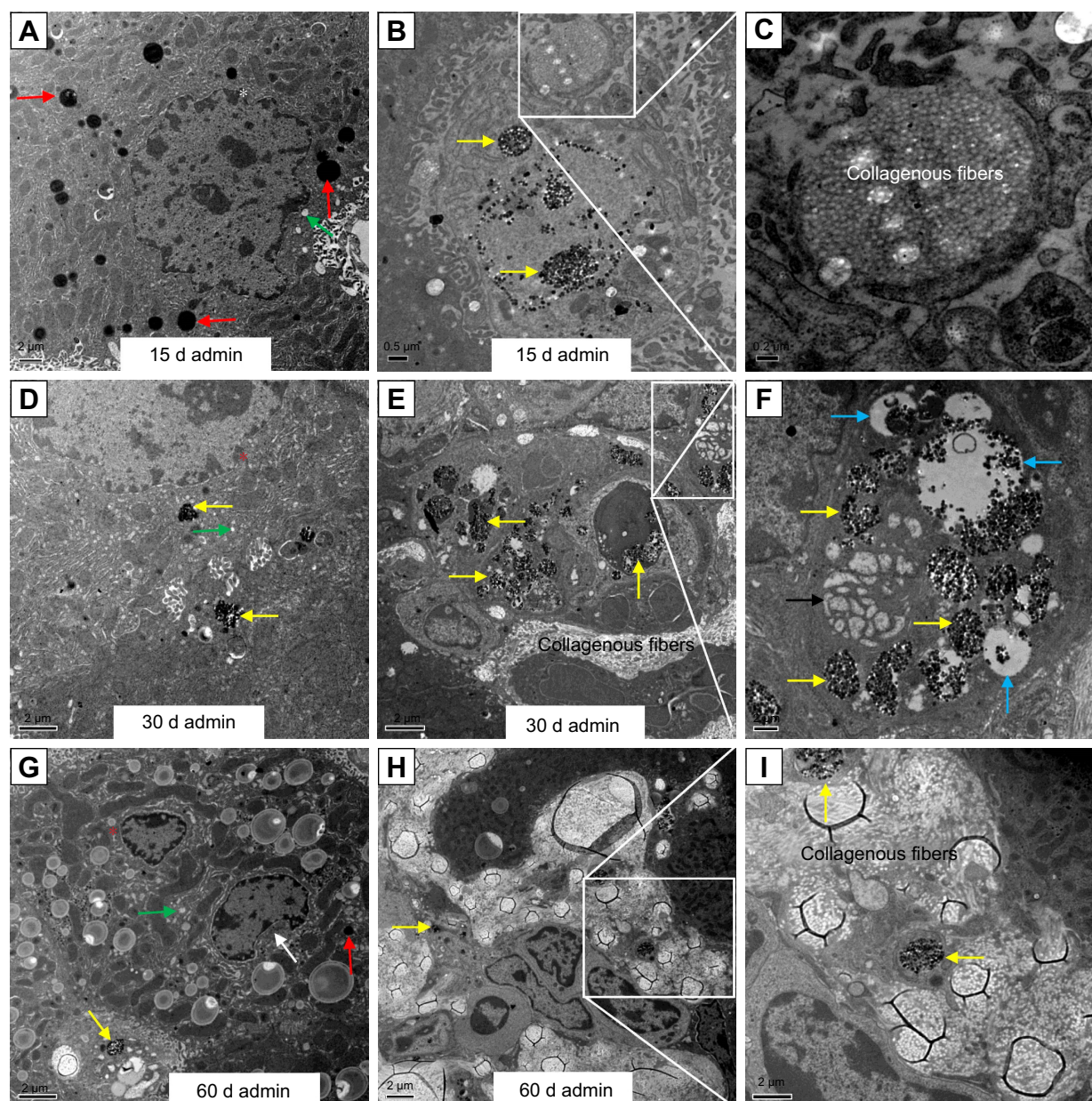
Figure 6 Ultrastructural changes in the liver of the SiO$_2$ NP treated mice at days 15, 30, and 60.

Notes: (**A**) Nuclear membrane distorted (white star), vacuolization (green arrows), and lipid droplet formation (red arrows) in the hepatocytes induced by the SiO$_2$ NPs in the liver at day 15 (5 K). (**B**) SiO$_2$ NPs (yellow arrows) in the hepatic sinusoid with proliferation of the collagen fibers starting at day 15 (8 K). (**C**) Magnification of the collagen fibers (25 K). (**D**) Nuclear membrane indentation with chromatin margination (red stars) and vacuolization (green arrows) in the hepatocytes in the liver at day 30 (8 K). (**E**) Hepatic granuloma mainly consisted of different kinds of cells at day 30 (4 K), (**F**) lamellar body-like structure formation (black arrow) and vacuolization (blue arrows) in the granuloma at day 30 (10 K). (**G**) Chromatin margination (red star), crescent-shaped nucleus (white arrow), and lipid droplet formation (red arrow) in the cytoplasm as well as vacuolization (green arrow) in the hepatocytes in the liver at day 60 (2.5 K). (**H**) Fibrotic granuloma induced by SiO$_2$ NPs at day 60 (3 K). (**I**) Magnification of the SiO$_2$ NPs surrounded by the white collagen fibers (8 K).

Abbreviations: admin, administration; SiO$_2$ NPs, silica nanoparticles.

TGF-β$_1$/Smad3 pathway protein expressions

Figure 10 showed the changes of TGF-β$_1$/Smad3 pathway protein expressions in the livers induced by SiO$_2$ NPs at day 30 and day 60. As shown in Figure 10A, intravenous administration of SiO$_2$ NPs induced upregulation of protein expression of TGF-β$_1$, Smad3, and p-Smad3 in the livers

at day 30 and day 60. In order to confirm the results of Western blotting, we conducted immunohistochemical staining of p-Smad3 in the liver sections of mice. As shown in Figure 10B and C, in the liver sections of control mice, p-Smad3 was mainly expressed in the nucleus of hepatocytes with large nucleus or binucleated, while in the livers of SiO$_2$ NP treated mice, p-Smad3 expression was observed not
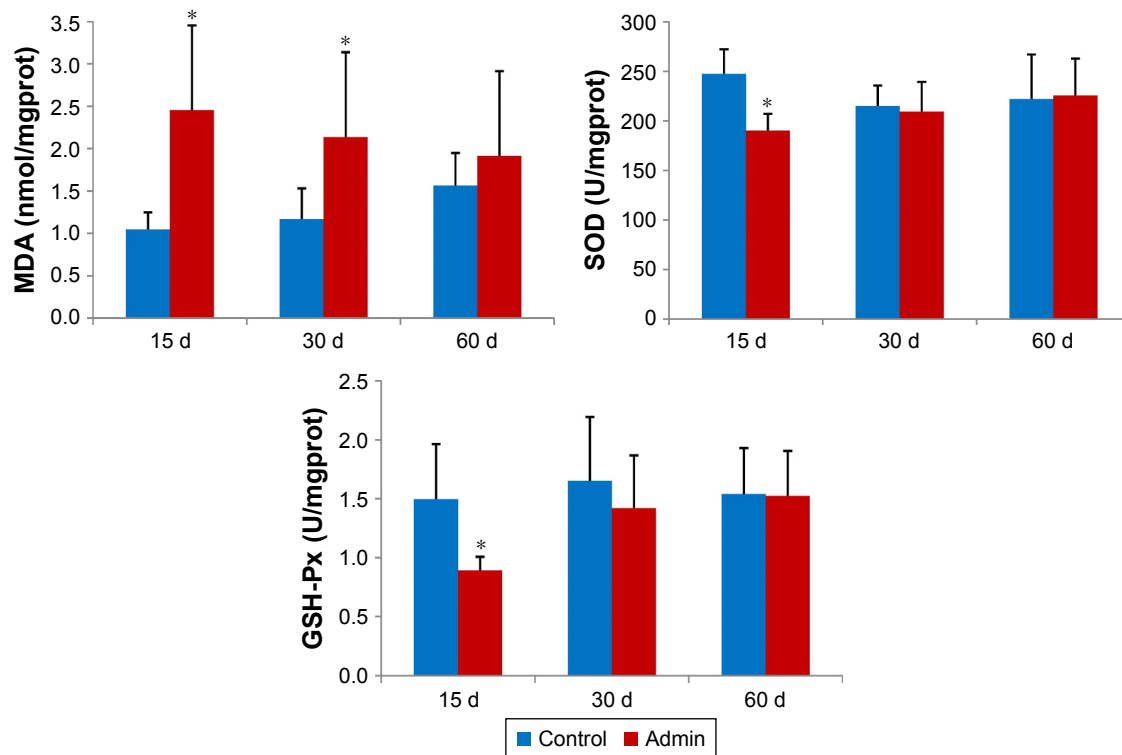
Figure 7 Levels of MDA, SOD, and GSH-Px in the liver of mice treated with the SiO_2 NPs at days 15, 30, and 60.
Notes: Data are expressed as mean ± SD (n=6). *$P<0.05$ compared with control group using independent sample t-test.
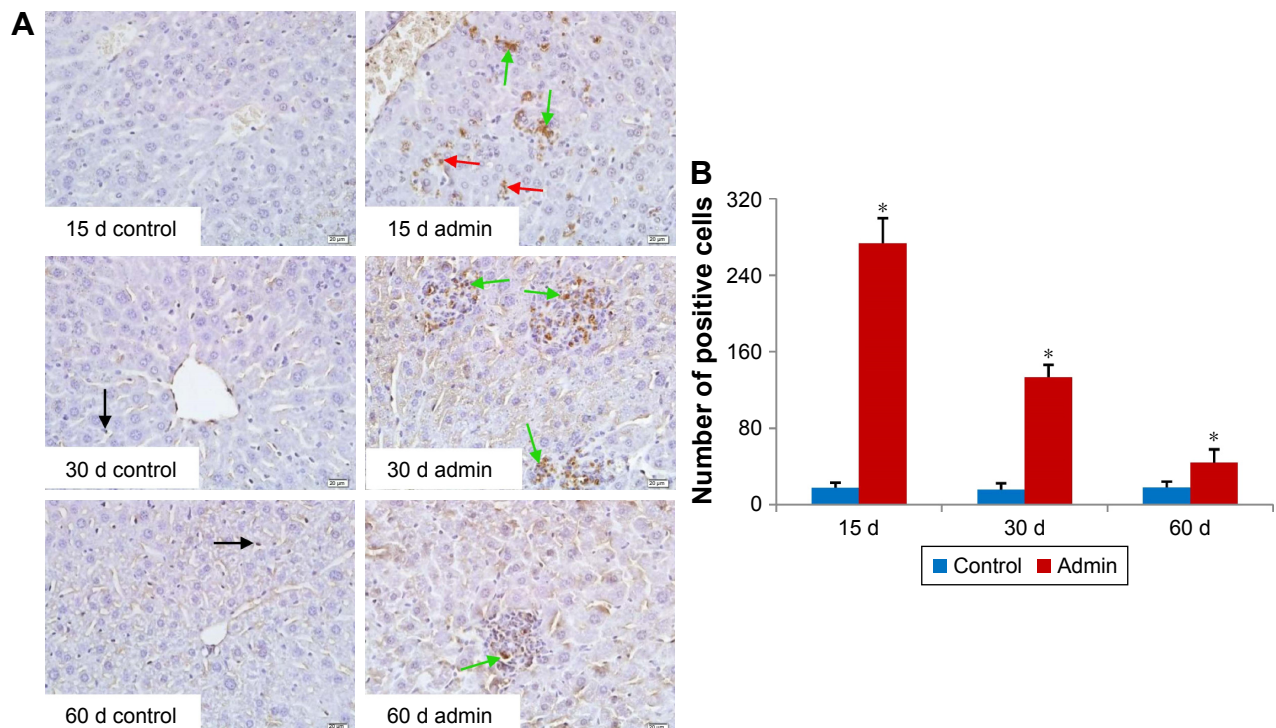**Abbreviations:** admin, administration; SiO_2 NPs, silica nanoparticles.

Figure 8 Apoptosis of the liver induced by SiO_2 NPs in mice at days 15, 30, and 60.
Notes: (**A**) Representative liver sections taken from the control mice and the SiO_2 NP treated mice at 400× magnification. Black arrows denote the TUNEL positive apoptotic cells in control group, while red arrows and green arrows denote the TUNEL positive apoptotic hepatocytes and TUNEL positive apoptotic cells in granulomas in the SiO_2 NP treated mice, respectively. (**B**) The number of TUNEL positive cells increased in the SiO_2 NPs treated mice at days 15, 30, and 60. *$P<0.05$ compared with control group using independent sample t-test. Data are representative of at least six mice. Scale bars =20 μm.
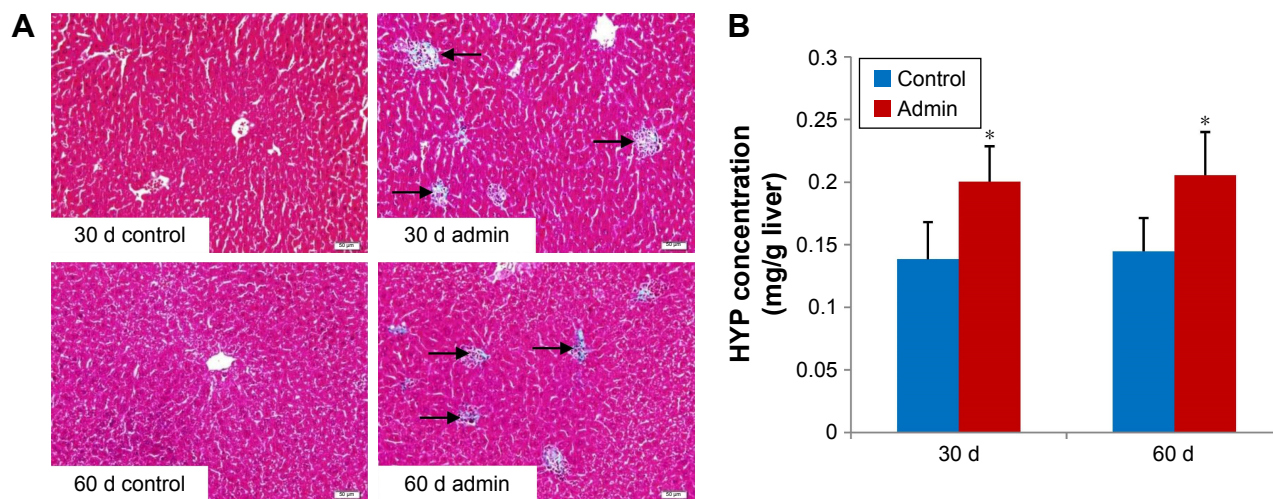**Abbreviations:** admin, administration; SiO_2 NPs, silica nanoparticles.

Figure 9 Collagen fiber level in the liver.

Notes: (**A**) Photographs of liver sections stained with Masson's trichrome. Black arrows denote the collagen fibers appearing in granulomas in the SiO$_2$ NP treated mice at days 30 and 60. Data are representative of at least six mice. (**B**) The hydroxyproline level in the liver of the SiO$_2$ NP treated mice at days 30 and 60. The hydroxyproline level in SiO$_2$ NP treated groups was significantly increased compared with control groups. *$P<0.05$ compared with control group using independent sample t-test. Data are representative of at least six mice. Scale bar =20 μm.

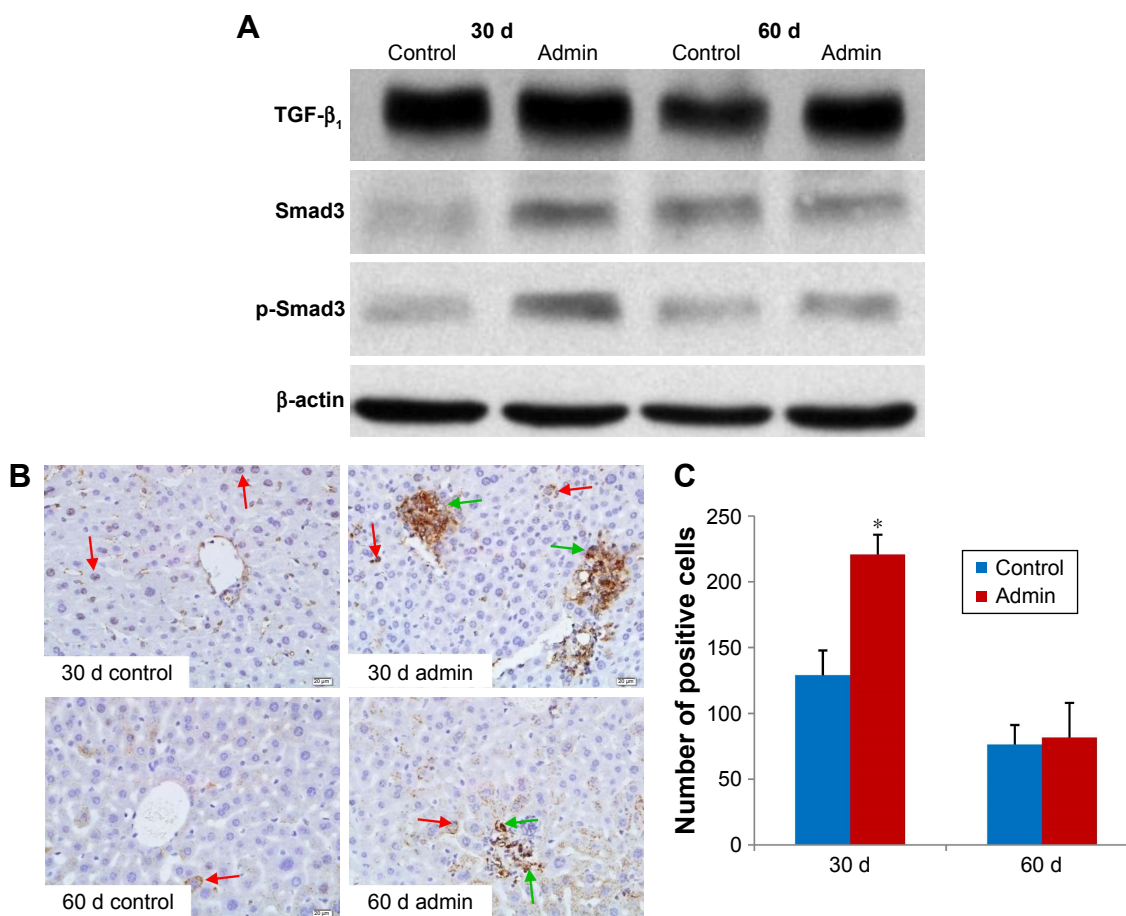**Abbreviations:** Admin, administration; SiO$_2$ NPs, silica nanoparticles; HYP, hepatic hydroxyproline.

Figure 10 TGF-β$_1$/Smad3 pathway protein expression in liver.

Notes: (**A**) Western blotting analysis of TGF-β$_1$, Smad3, and p-Smad3 protein expression in liver of SiO$_2$ NP treated mice at days 30 and 60. Data are representative of at least three mice. (**B**) Immunohistochemistry staining of p-Smad3 in liver of the SiO$_2$ NP treated mice at days 30 and 60. Representative liver sections taken from the control mice and the SiO$_2$ NP treated mice at 400× magnification. Red arrows denote the p-Smad3 positive hepatocytes, while green arrows denote the p-Smad3 positive cells in granulomas in SiO$_2$ NP treated mice. (**C**) The number of p-Smad3 positive cells increased in SiO$_2$ NP treated mice at day 30 and day 60. *$P<0.05$ compared with control group using independent sample t-test. Data are representative of at least six mice.

Abbreviations: Admin, administration; SiO$_2$ NPs, silica nanoparticles.

only in the hepatocytes, but also in the KCs and HSCs or myofibroblast in the hepatic sinusoid or in the granulomas.

Discussion

In the present study, intravenous injection of SiO$_2$ NPs induced hepatic granuloma formation, oxidative damage, and apoptosis. Oxidative damage and apoptosis activated TGF-β$_1$/Smad3 signaling pathway and then resulted in hepatic fibrogenesis. This study provided important information for the hepatic toxicity evaluation and the biomedical and pharmaceutical application of SiO$_2$ NPs.

The most important observation in the present study is liver fibrosis induced by intravenous exposure to SiO$_2$ NPs. The liver fibrosis induced by SiO$_2$ NPs was initiated from the granuloma formation. Granuloma is an innate immune response designed to isolate xenobiotics initiated by the phagocytosis of macrophages. Granuloma induced by nanomaterials through different exposure routes, including intratracheal instillation and intravenous injection, has been reported by several studies.[9,16,17] In the previous study, we demonstrated that SiO$_2$ NPs induced granuloma in the liver in a dose-dependent manner.[7] In the early phase, the granuloma consists of different kinds of cells including macrophages, lymphocytes, and neutrophils, but in the late phase, during the HSC and fibroblast activation, accumulation of excessive extracellular matrix (ECM) contributes to the progression of liver fibrosis.

Oxidative damage is recognized as the most important toxic mechanism of nanomaterials, including SiO$_2$ NPs. It is well known that SiO$_2$ NPs induce ROS production and oxidative damage in different cell lines in a dose-dependent manner.[12,18,19] This study demonstrated increased MDA level and decreased SOD and GSH-Px activities in the liver induced by the deposition of SiO$_2$ NPs, indicating the elevation of ROS production and oxidative stress caused by SiO$_2$ NPs. Because of the unsaturated bond and silicon-bonded hydroxyl groups on the particle surface, SiO$_2$ NPs are prone to induce ROS generation and oxidative damage.[20] Our previous studies indicated that SiO$_2$ NPs could enter the cells and induce oxidative stress in different cell lines in a dose- and size-dependent manner.[12,18,19] Park and Park reported that SiO$_2$ NPs induced ROS generation and GSH levels decreased in macrophage cell line RAW 264.7 cells.[21] Meanwhile, there is a substantial body of evidence indicating that oxidative damage is a common pathological feature of fibrosis, and plays an important role in the development of fibrogenesis under different pathological conditions.[22] ROS could enhance the gene expression of TGF-β$_1$ which is considered to be the most potent profibrogenic cytokine, and

plays important roles in the development of fibrogenesis, and induces deposition of ECM in tissue injuries in many organs such as the heart, the lungs, the kidney, and the liver.[23–26] ROS also mediates a series of profibrogenic effects of TGF-β$_1$ including fibroblast migration and maintaining the myofibroblast phenotype.[27,28] Azad et al found that ROS mediated fibroblast activation and collagen composition was induced by carbon nanotubes.[29] In the present study, the oxidative damage induced by SiO$_2$ NPs may trigger the expression of TGF-β$_1$, thus activating the HSCs and fibroblasts, and contributing to the pathogenesis of liver fibrosis.

Accumulating evidence indicates that apoptosis may be linked to the development of fibrogenesis directly. It was shown that inhibition of caspase to reduce apoptosis could ameliorate tissue fibrosis.[30] In this study, we observed that SiO$_2$ NPs induced more TUNEL-positive hepatocytes and KCs in the experimental groups. It has been reported that persistent hepatocyte apoptosis led to liver fibrosis.[31] The apoptotic hepatocyte cells would be effectively and rapidly engulfed by KCs in the liver, and the accumulation of apoptotic bodies in KCs would enhance the proinflammatory cytokine TNF-α in KCs, thereby speeding up hepatocyte apoptosis and inducing hepatic inflammation.[32] Besides, phagocytosis of apoptotic hepatocytes would promote generation of TGF-β$_1$ and thus accelerate liver fibrosis. We still observed prominent KC apoptosis in this study, which was also reported to be associated with liver fibrosis, through in turn activating HSCs by releasing TGF-β$_1$.[33]

TGF-β$_1$ has been shown to stimulate the proliferation and activation of fibroblasts and HSCs in the liver. Smad3 is the central mediator conveying signals from receptors for TGF-β$_1$ to the nucleus, and p-Smad3 is a mark of activation for the TGF-β$_1$/Smad3 signaling pathway.[34–36] The activation of TGF-β$_1$/Smad3 signaling pathway led to the expression of profibrogenic genes.[37] So above all, in the present study, intravenous injection of SiO$_2$ NPs induced oxidative damage and apoptosis in the liver, which activated TGF-β$_1$/Smad3 signaling pathway and contributed to liver fibrosis. But the mechanism needs to be further explored.

Besides, when we studied the toxicity and mechanism of nanoparticles, we should also pay attention to reducing the toxicity of nanoparticles. Surface modification of nanoparticles has been recognized as one important way to increase the stability and reduce the toxicity of nanoparticles. It was reported that SiO$_2$ NPs modified with amine functional groups induced less serious lung inflammation and possessed better biocompatibility.[38] Lu et al found that amino and carboxyl surface modification mitigated the hepatic toxicity of SiO$_2$ NPs.[39] However, there is a lack of more meticulous

and systemic studies about the effects of surface modification on the toxicity of SiO$_2$ NPs. Indeed, we are conducting a comparative study of PEG-SiO$_2$ NPs and naked SiO$_2$ NPs in our lab.

In the present study, the level of hepatic fibrosis gradually deteriorated as the granulomas, oxidative damage, and apoptosis in the liver was gradually relieved within the observation period. Further study is needed to explore the related mechanisms. It is also noteworthy that liver function remained in a deteriorated condition in the SiO$_2$ NP treated mice at the end of this study. So above all, in biomedical and pharmaceutical application, attention should be paid to the profibrogenic effects and hepatic toxicity of amorphous SiO$_2$ NPs.

Conclusion

In conclusion, we investigated the hepatic fibrosis and related mechanisms induced by intravenous injection of SiO$_2$ NPs in vivo. In the observation period, SiO$_2$ NPs were distributed in the hepatocytes, KCs, HSCs, and fibroblast cells, and induced oxidative damage and apoptosis, thus activating the TGF-β_1/Smad3 signaling pathway, thereby activating HSCs and fibroblast cells to initiate and promote liver fibrosis. Thus, the impairment of liver function and profibrogenic effects induced by SiO$_2$ NPs in biomedical and pharmaceutical application is noteworthy. It was confirmed that SiO$_2$ NPs could cause fibrosis via oxidative stress and apoptosis for the first time. Further mechanisms in hepatic fibrosis, and how to alleviate or avoid liver injury in intravenous exposure to SiO$_2$ NPs needs to be studied in the near future.

Acknowledgment

Disclosure

The authors report no conflicts of interest in this work.

References

1. National Institute of Environmental Health Sciences, National Institutes of Health, U.S. Department of Health and Human Services. National Toxicology Program (NTP). *Chemical Information Review Document for Silica Flour [CAS No.14808-60-7]*. Research Triangle Park, NC: National Institute of Environmental Health Sciences, National Institutes of Health, U.S. Department of Health and Human Services; 2009. Available from: https://ntp.niehs.nih.gov/ntp/noms/support_docs/silicaflour_oct2009.pdf. Accessed June 22, 2017.
2. Neophytou AM, Yiallouros P, Coull BA, et al. Particulate matter concentrations during desert dust outbreaks and daily mortality in Nicosia, Cyprus. *J Expo Sci Environ Epidemiol*. 2013;23(3):275–280.
3. OECD.org [homepage on the Internet]. Series on the safety of manufactured nanomaterials No. 27-ENV/JM/MONO(2010)46. OECD; 2010. Available from: http://www.oecd.org/science/nanosafety/. Accessed June 22, 2017.
4. Saba TM. Physiology and physiopathology of the reticuloendothelial system. *Arch Intern Med*. 1970;126(6):1031–1052.
5. Linkov I, Satterstrom FK, Corey LM. Nanotoxicology and nanomedicine: making hard decisions. *Nanomedicine*. 2008;4(2):167–171.
6. Kumar R, Roy I, Ohulchanskky TY, et al. In vivo biodistribution and clearance studies using multimodal organically modified silica nanoparticles. *ACS Nano*. 2010;4(2):699–708.
7. Yu Y, Li Y, Wang W, et al. Acute toxicity of amorphous silica nanoparticles in intravenously exposed ICR mice. *PLoS One*. 2013;8(4):e61346.
8. Nishimori H, Kondoh M, Isoda K, Tsunoda S, Tsutsumi Y, Yagi K. Histological analysis of 70-nm silica particles-induced chronic toxicity in mice. *Eur J Pharm Biopharm*. 2009;72(3):626–629.
9. Nishimori H, Kondoh M, Isoda K, Tsunoda S, Tsutsumi Y, Yagi K. Silica nanoparticles as hepatotoxicants. *Eur J Pharm Biopharm*. 2009; 72(3):496–501.
10. van der Zande M, Vandebriel RJ, Groot MJ, et al. Sub-chronic toxicity study in rats orally exposed to nanostructured silica. *Part Fibre Toxicol*. 2014;11:8.
11. Liu T, Li L, Teng X, et al. Single and repeated dose toxicity of mesoporous hollow silica nanoparticles in intravenously exposed mice. *Biomaterials*. 2011;32(6):1657–1668.
12. Sun L, Li Y, Liu X, et al. Cytotoxicity and mitochondrial damage caused by silica nanoparticles. *Toxicol In Vitro*. 2011;25(8):1619–1629.
13. Iwaisako K, Hatano E, Taura K, et al. Loss of Sept4 exacerbates liver fibrosis through the dysregulation of hepatic stellate cells. *J Hepatol*. 2008;49(5):768–778.
14. Kivirikko KI, Laitinen O, Prockop DJ. Modifications of a specific assay for hydroxyproline in urine. *Anal Biochem*. 1967;19(2):249–255.
15. Duan J, Yu Y, Yu Y, et al. Silica nanoparticles enhance autophagic activity, disturb endothelial cell homeostasis and impair angiogenesis. *Part Fibre Toxicol*. 2014;11:50.
16. Tseng MT, Lu X, Duan X, et al. Alteration of hepatic structure and oxidative stress induced by intravenous nanoceria. *Toxicol Appl Pharmacol*. 2012;260(2):173–182.
17. Osmond-McLeod MJ, Poland CA, Murphy F, et al. Durability and inflammogenic impact of carbon nanotubes compared with asbestos fibres. *Part Fibre Toxicol*. 2011;8:15.
18. Li Y, Sun L, Jin M, et al. Size-dependent cytotoxicity of amorphous silica nanoparticles in human hepatoma HepG2 cells. *Toxicol In Vitro*. 2011;25(7):1343–1352.
19. Duan J, Yu Y, Yu Y, et al. Silica nanoparticles induce autophagy and endothelial dysfunction via the PI3K/Akt/mTOR signaling pathway. *Int J Nanomedicine*. 2014;9:5131–5141.
20. Napierska D, Thomassen LC, Lison D, Martens JA, Hoet PH. The nanosilica hazard: another variable entity. *Part Fibre Toxicol*. 2010; 7(1):39.
21. Park EJ, Park K. Oxidative stress and pro-inflammatory responses induced by silica nanoparticles in vivo and in vitro. *Toxicol Lett*. 2009; 184(1):18–25.
22. Liu RM, Gaston Pravia KA. Oxidative stress and glutathione in TGF-beta-mediated fibrogenesis. *Free Radic Biol Med*. 2010;48(1):1–15.
23. Yoshioka K, Takemura T, Murakami K, et al. Transforming growth factor-β protein and mRNA in glomeruli in normal and diseased human kidneys. *Lab Invest*. 1993;68(2):154–163.
24. Friedman SL. Seminars in medicine of the Beth Israel Hospital, Boston. The cellular basis of hepatic fibrosis. Mechanisms and treatment strategies. *N Engl J Med*. 1993;328(25):1828–1835.
25. Border WA, Noble NA. Transforming growth factor β in tissue fibrosis. *N Engl J Med*. 1994;331(19):1286–1292.

26. Coker RK, Laurent GJ. Pulmonary fibrosis: cytokines in the balance. *Eur Respir J*. 1998;11(6):1218–1221.

27. Jiang F, Liu GS, Dusting GJ, Chan EC. NADPH oxidase-dependent redox signaling in TGF-β-mediated fibrotic responses. *Redox Biol*. 2014; 2:267–272.

28. Liu XX, Zhou HJ, Cai L, et al. NADPH oxidase-dependent formation of reactive oxygen species contributes to transforming growth factor β1-induced epithelial-mesenchymal transition in rat peritoneal meso-thelial cells, and the role of astragalus intervention. *Chin J Integr Med*. 2014;20(9):667–674.

29. Azad N, Iyer AK, Wang L, Liu Y, Lu Y, Rojanasakul Y. Reactive oxy-gen species-mediated p38 MAPK regulates carbon nanotube-induced fibrogenic and angiogenic responses. *Nanotoxicology*. 2013;7(2): 157–168.

30. Lee CG, Cho SJ, Kang MJ, et al. Early growth response gene 1-mediated apoptosis is essential for transforming growth factor beta1-induced pulmonary fibrosis. *J Exp Med*. 2004;200(3):377–389.

31. Takehara T, Tatsumi T, Suzuki T, et al. Hepatocyte-specific disruption of Bcl-xL leads to continuous hepatocyte apoptosis and liver fibrotic responses. *Gastroenterology*. 2004;127(4):1189–1197.

32. Guicciardi ME, Gores GJ. Apoptosis: a mechanism of acute and chronic liver injury. *Gut*. 2005;54(7):1024–1033.

33. Liu C, Tao Q, Sun M, et al. Kupffer cells are associated with apoptosis, inflammation and fibrotic effects in hepatic fibrosis in rats. *Lab Invest*. 2010;90(12):1805–1816.

34. Shi Y, Massagué J. Mechanisms of TGF-β signaling from cell mem-brane to the nucleus. *Cell*. 2003;113(6):685–700.

35. Kubiczkova L, Sedlarikova L, Hajek R, Sevcikova S. TGF-β – an excellent servant but a bad master. *J Transl Med*. 2012;10:183.

36. Chen JL, Shang QH, Hu W, Liu C, Mao WH, Liu HQ. Role of TGF-β1/Smads pathway in carotid artery remodeling in renovascular hyperten-sive rats and prevention by Enalapril and Amlodipine. *J Geriatr Cardiol*. 2012;9(2):185–191.

37. Dooley S, ten Dijke P. TGF-β in progression of liver disease. *Cell Tissue Res*. 2012;347(1):245–256.

38. Morris AS, Adamcakova-Dodd A, Lehman SE, et al. Amine modifica-tion of nonporous silica nanoparticles reduces inflammatory response following intratracheal instillation in murine lungs. *Toxicol Lett*. 2016;241:207–215.

39. Lu X, Ji C, Jin T, Fan X. The effects of size and surface modification of amorphous silica particles on biodistribution and liver metabolism in mice. *Nanotechnology*. 2015;26(17):175101.